Effects of Mg-doping concentration on the characteristics of InGaN based solar cells*

LU Gang (路纲), **WANG Bo** (王波), **and GE Yun-wang** (葛运旺)**

Department of Electrical Engineering and Automation, Luoyang Institute of Science and Technology, Luoyang 471023, China

(Received 26 May 2015)

A major challenge in GaN based solar cell design is the lack of holes compared with electrons in the multiple quantum wells (MQWs). We find that GaN based MQW photovoltaic devices with five different Mg-doping concentrations of 0 cm^{-3}, 5×10^{17} cm^{-3}, 2×10^{18} cm^{-3}, 4×10^{18} cm^{-3} and 7×10^{18} cm^{-3} in GaN barriers can lead to different hole concentrations in quantum wells (QWs). However, when the Mg-doping concentration is over 1×10^{18} cm^{-3}, the crystal quality degrades, which results in the reduction of the external quantum efficiency (*EQE*), short circuit current density and open circuit voltage. As a result, the sample with a slight Mg-doping concentration of 5×10^{17} cm^{-3} exhibits the highest conversion efficiency.

Document code: A **Article ID:** 1673-1905(2015)05-0348-4

DOI 10.1007/s11801-015-5100-4

Nowadays, InGaN ternary alloys have drawn great attention in the field of optoelectronics due to their unique physical characteristics, including excellent radiation resistance, good thermal conductivity, large absorption coefficients (~10^5 cm^{-1})[1] and wide band gap (varying from 0.64 eV to 3.4 eV) covering most of the solar spectrum[2-7], which makes them suitable for producing solar cells.

Until now, there are several difficulties in the fabrication of InGaN based solar cells with high efficiency. Firstly, the hole mobility in the InGaN material is about 10 $cm^2/(V\cdot s)$, but the electron mobility in the InGaN material is about 100 $cm^2/(V\cdot s)$, so there is relatively large lack of holes in InGaN based optoelectronic devices. Secondly, InGaN layers with higher indium (In) proportion are needed to fabricate InGaN-based multijunction solar cells with nearly ideal band gaps for maximum solar energy conversion efficiency. The earlier theoretical calculation indicated that an active material system with power conversion efficiency greater than 50% could be achieved by InGaN alloys with In proportion of about 40%[5]. Unfortunately, the fabrication of solar cells with large In proportion remains a challenge, because of the large lattice mismatch between indium nitride and gallium nitride. When the layer thickness and/or In proportion of InGaN alloys increase, In clusters in InGaN films easily lead to phase separation, which results in the lower open circuit voltages (V_{oc}) compared with theoretical values, the low fill factors (*FFs*) and degradation of the short-circuit current density (J_{sc})[6-10].

To partially overcome the In incorporation limitation in thick layers, many researchers have adopted multiple quantum wells (MQWs) or superlattice absorbing layers[11-13]. InGaN based MQW optical devices can not only obtain higher crystal quality of InGaN absorption layers embedded between GaN barriers, but also optimize V_{oc} and J_{sc} independently by adjusting parameters of quantum barrier and well materials[14]. However, up to now, the energy harvesting efficiency of these devices is not comparable to the theoretical value of devices with a corresponding In mole fraction. To improve the performance of InGaN-based photovoltaic device, it is urgent to implement the in-depth investigation and the optimization of the construction, especially the optimization of the active region.

Mg doping of InGaN quantum wells can increase the hole concentration and alleviate the electrostatic field in the InGaN/GaN MQWs. The alleviation of electrostatic field is good for increasing the In incorporation in InGaN alloy. In this paper, we investigate the effect of Mg doping on the characteristics of InGaN based solar cells.

Fig.1(a) shows the structure of the solar cells. The MQW photovoltaic devices were deposited on c-plane sapphire by Thomas Swan metal-organic chemical vapor deposition (MOCVD). A 25 nm-thick low-temperature GaN nucleation layer, a 2 μm-thick undoped GaN layer and a 2 μm-thick Mg-doped n-type GaN with doping concentration of 1×10^{19} cm^{-3} were grown on the sapphire in sequence. Next the MQW absorbing layer was grown, which consists of 15 periods of $In_{0.2}Ga_{0.8}N$/GaN quantum

* This work has been supported by the Key Scientific Research Project of Higher Education of Henan Province (No.15A510033).

** E-mail: gyw789@foxmail.com

well layers with thickness of ~3 nm and GaN quantum barrier (QB) layers with thickness of ~6 nm. The light emitting layer was a 160 nm-thick p-type GaN layer (5×10^{17} cm^{-3}). Five groups of samples (A, B, C, D and E), which were nominally identical apart from different Mg-doping concentrations in GaN barrier of 0 cm^{-3}, 5×10^{17} cm^{-3}, 2×10^{18} cm^{-3}, 4×10^{18} cm^{-3} and 7×10^{18} cm^{-3}, were grown specifically to study the influence of Mg doping in the GaN barriers on the characteristics of InGaN based solar cells. The barrier doping concentration is determined by Hall effect measurement.

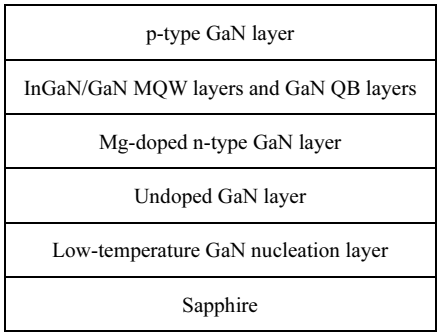

Fig.1 Cross-sectional schematic diagram of the device structure

After the epitaxy growth, the samples were characterized by a high-resolution X-ray diffractometer (HRXRD). Some devices were also manufactured into solar cells using standard lithography procedures. The area of the solar cell was designed to be 2 mm×2 mm and without any antireflective coating. The external quantum efficiency (*EQE*) was measured by using an Xe broadband light source coupled with an Oriel 260 monochromator and adjusted by a reference standard photodetector. The dark and light current densities versus voltage (*J-V*) were measured by a Keithley 2400 source meter. The devices were illuminated under 100 mW/cm^2 AM1.5G.

The X-ray diffraction (XRD) spectra of all samples are shown in Fig.2(a). The similar peak positions indicate that the average composition and the period of MQW regions are similar for all samples. It can be obtained by the X-ray simulation program that the In proportion, well and barrier thicknesses are estimated to be around 20%, 3 nm and 6 nm, respectively. The full width at half maximum (*FWHM*) values at the first order diffraction peak of samples A–E are 219″, 226″, 270″, 317″ and 318″, respectively. Such an observation suggests that the crystal characteristics of slightly doped sample B are comparable with those of the undoped sample A, but the crystal quality degrades with the further increase of barrier doping.

The reciprocal space maps of the (105) reflection were also measured for all samples. A slight shift of MQW diffraction peak compared with that of the GaN layer can be observed in the map of each sample. The lateral shift is very small in samples A (not shown here) and B (shown in Fig.2(b)), but becomes obvious in highly doped samples as the map for sample E shown in Fig.2(c). The results indicate that coherency strain of the MQW is not sensitive to the slight Mg doping in barrier, but may be aggravated by heavy doping (when Mg-doping concentration is over 2×10^{18} cm^{-3}). The coherency strain accumulates with the increase of Mg-doping concentration, which finally results in lattice relaxation and induces defects. As a result, the crystal quality degrades with heavy Mg doping, which is consistent with the variation of *FWHM* in XRD (ω-2θ) curves.

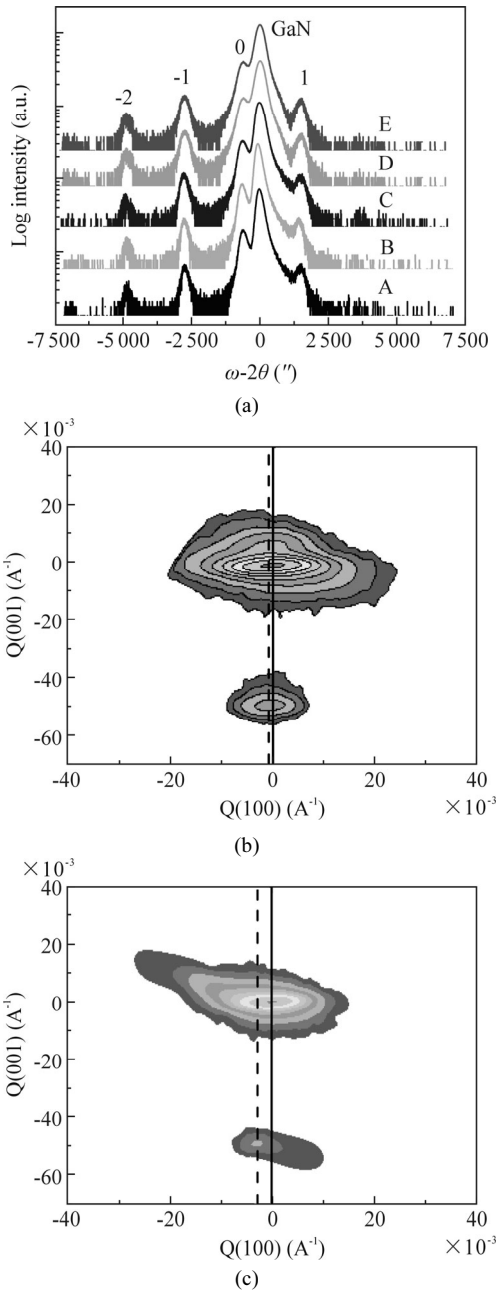

Fig.2 (a) The (0002) XRD *ω-2θ* curves for all devices; Reciprocal space maps about the asymmetric (105) reflection for (b) sample B and (c) sample E

The *EQE* curves of samples A and B are shown in Fig.3. It is clearly shown that the primary response of all

samples ranges from 420 nm to 500 nm. The variations of *EQE* of samples A and B with incident photon wavelength have similar trend over the whole response range, but the *EQE* values are quite different due to different doping concentrations, especially in the wavelength range longer than 440 nm, which are associated with absorption in the MQWs. The peak value of *EQE* at about 375 nm is improved from 30% (undoped sample A) to 33.9% (5×10^{17} cm^{-3} Mg doped sample B). The result indicates that the *EQE* of InGaN based MQW cells may be enhanced by slight Mg doping in barrier, while weakened by heavy Mg doping. The decrease in the region of λ<440 nm may be explained by the absorption of light in the Mg-doped gallium nitride barrier layers[15].

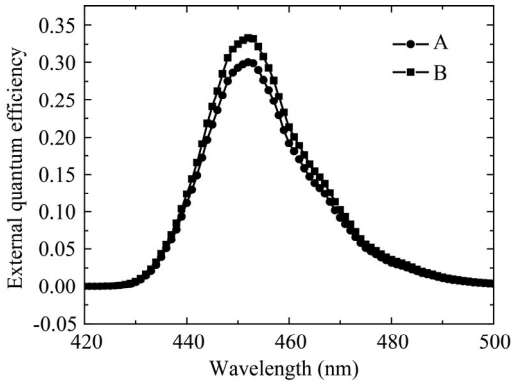

Fig.3 Dependence of *EQE* on wavelength for samples A and B

Fig.4(a) depicts the *J-V* curves of the four MQW photovoltaic devices under dark condition. With identical current injection, it is found that forward voltages decrease from sample A to sample D with the increase of Mg-doping concentration. The result clearly demonstrates that the series resistance (R_s) decreases as the Mg-doping concentration in GaN barrier layers increases, which means that the transport properties of the MQW layers can be improved by the Mg-doped barrier layers. With good crystal quality and better transport property, the collection efficiency of photogenerated carriers in slightly doped sample is improved, and higher *EQE* is obtained. On the other hand, the doped samples display larger leakage current with increase of doping concentration. Specifically, the leakage current of slightly doped sample B (5×10^{17} cm^{-3}) is comparable but still larger than that of sample A, while the leakage currents of other samples are much larger. The leakage current may take place by tunneling through the threading dislocations[16]. The photogenerated carriers could be easily captured by the high density defects. As a result, the *EQE* decreases with heavy Mg-doping in barrier.

Fig.4(b) shows the series resistance (R_s) and shunt resistance (R_{sh}) as a function of Mg-doping concentration in barrier. The shunt resistance exhibits nearly a linear decreasing relationship with Mg-doping concentration. It is known that R_{sh} is mainly caused by short circuit pathways, such as threading dislocations (TDs)[17], thus the linear relationship agrees well with the XRD and dark *J-V* measurement results. On the other hand, slight doping (5×10^{17} cm^{-3}) almost reduces the shunt resistance by half from sample A to sample B, but the effect becomes inconspicuous when the doping concentration is further increased. However, the value of R_s is still lager compared with that in Ref.[18].

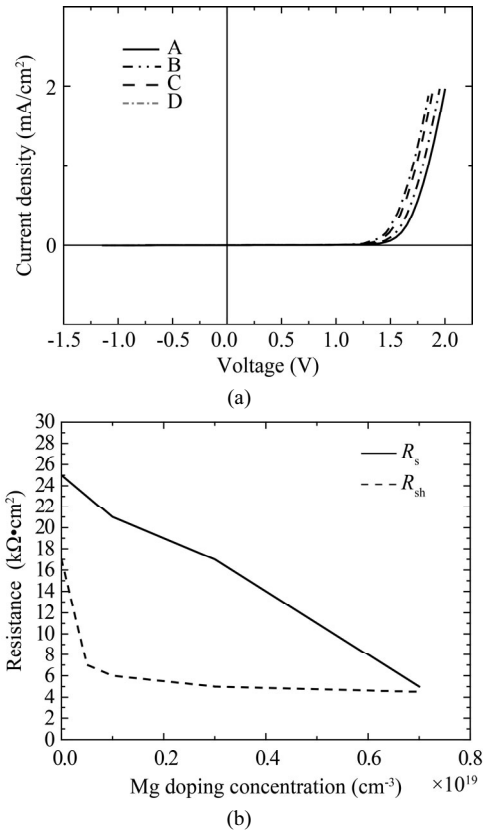

Fig.4 (a) Current density versus voltage of the InGaN based MQW photovoltaic devices of samples A–D in dark; (b) Series resistance and shunt resistance versus the Mg doping concentration for all samples

Tab.1 presents a summary of J_{sc}, V_{oc} and *FF* for devices with different doping concentrations. Higher doping concentration results in further degradation of electrical characteristics of InGaN/GaN MQW solar cells. The variation trend of J_{sc} can be explained as follows. By considering resistive losses due to R_s and R_{sh}, the *I-V* equation of the solar cell can be expressed as

$$I(V) = I_{SC} - I_0\left\{\exp\left[\frac{e(V+IR_s)}{nkT}\right]-1\right\}-\frac{V+IR_s}{R_{sh}}, \quad (1)$$

where the multiplier I_0 is the saturation current, n in the denominator of the exponent is the ideality factor, and $I(0)$ corresponds directly to I_{sc}. According to Eq.(1), $I(V)$ current measured by the external circuit increases when R_s decreases, while declines when R_{sh} reduces. Taking the decreases of R_s and R_{sh} into account, as discussed above,

the increased J_{sc} of sample B indicates that the optimization of R_s is superior to the degradation of R_{sh}. However, the degradation of R_{sh} becomes dominant in highly doped samples. The leakage current related nonradiative centers[19] lead to a short diffusion length of the carriers, resulting in the recombination of photogenerated carriers before they can be collected[20, 21], which finally leads to the decrease of J_{sc}. On the other hand, V_{oc} slightly decreases from 1.75 V to 1.74 V, and then decreases monotonically to 1.17 V. It is known that V_{oc} of the photovoltaic device is decided mainly by the barrier, the recombination in the wells and the QW/QB interface energy difference. Non-radiative recombination effects largely influence the value of V_{oc}[22], and in this way the degradation of crystal quality due to heavy Mg doping leads to the decrease of V_{oc}. By optimizing doping methods, like gradient-doping or moderately doping a few nanometers in the centers of the barriers, we may avoid poor QW/QB interfaces and the degradation of crystal quality, and can guarantee the good transport property at the same time. We will conduct further research in the future.

The best performance of the devices is achieved by introducing slight Mg doping in GaN barriers. However, *EQE*, J_{sc} and V_{oc} are adversely affected by heavy Mg-doping in barrier. Therefore, barrier doping is an important factor in the design of InGaN/GaN MQW solar cells, and our experiment suggests that slight Mg-doping in GaN barriers is desirable. It is notable that the *FF* increases with increase of Mg-doping. Specifically, *FF* for sample E is increased by 30.8% compared with that of sample A. The results demonstrate that the *FF* of MQW solar cells can be improved by doping Mg in the GaN barriers, which is attributed to the better transport property of Mg doped MQWs.

Tab.1 Solar cell performances of samples A–E

Sample	V_{oc} (V)	J_{sc} (mA/cm^2)	*FF* (%)
A	1.75	0.50	40.39
B	1.74	0.75	39.03
C	1.54	0.34	42.19
D	1.37	0.20	46.49
E	1.17	0.15	51.83

In conclusion, the influence of Mg-doping concentration in GaN barrier on the performance of InGaN based MQW photovoltaic solar cells is analyzed. R_s decreases and *FF* increases remarkably as Mg-doping concentration in GaN barrier increases. These results are attributed to the improvement of the transport property by doping Mg in the GaN barriers. However, the crystal quality degrades as Mg-doping concentration increases, resulting in the reduction of *EQE*, J_{sc} and V_{oc}. As a result, the sample with a slight Mg-doping concentration of 5×10^{17} cm^{-3} exhibits the highest conversion efficiency.

References

[1] David A. and Grundmann M. J., Applied Physics Letters **97**, 033501 (2010).

[2] Nanishi Y., Saito Y. and Yamaguchi T., Japanese Journal of Applied Physics **42**, 2549 (2003).

[3] FU Yun-ying, DAI Li-ping, WANG Shu-ya and ZHANG Guo-jun, Optoelectronics Letters **9**, 278 (2013).

[4] Liu J., Wu Z. C. and Kuang S. P., Optoelectronics and Advanced Materials-Rapid Communications **7**, 343 (2013).

[5] Vos A. D., Endoreversible Thermodynamics of Solar Energy Conversion, Oxford: Oxford University Press, 90 (1992).

[6] Jani O., Ferguson I., Honsberg C. and Kurtz S., Applied Physics Letters **91**, 132117 (2007).

[7] K. A. S. M. Ehteshamul Haque, Optoelectronics Letters **9**, 177 (2013).

[8] Lai K. Y., Lin G. J., Lai Y. L., Chen Y. F. and He J. H., Applied Physics Letters **96**, 081103 (2010).

[9] Jampana B. R., Melton A. G., Jamil M. N., Faleev N., Opila R. L., Ferguson I. T. and Honsberg C. B., IEEE Electron Device Letters **31**, 32 (2010).

[10] Zeng S. W., Cai X. M. and Zhang B. P., IEEE Journal of Quantum Electronics **46**, 783 (2010).

[11] Dahal R., Pantha B., Li J., Li J. Y. and Jiang H. X., Applied Physics Letters **98**, 263504 (2011).

[12] Yang C. C., Sheu J. K., Liang X. W., Huang M. S., Lee M. L., Chang K. H., Tu S. J., Huang F. W. and Lai W. C., Applied Physics Letters **97**, 021113 (2010).

[13] Farrell R. M., Neufeld C. J., Cruz S. C., Lang J. R., Iza M., Keller S., Nakamura S., DenBaars S. P., Mishra U. K. and Speck J. S., Applied Physics Letters **98**, 201107 (2011).

[14] Dahal R., Li J., Aryal K., Lin J. Y. and Jiang H. X., Applied Physics Letters **97**, 073115 (2010).

[15] Wu L. W., Chang S. J., Wen T. C., Su Y. K., Chen J. F., Lai W. C., Kuo C. H., Chen C. H. and Sheu J. K., IEEE Journal of Quantum Electronics **38**, 446 (2002).

[16] Cao X. A., Stokes E. B., Sandvik P. M., LeBoeuf S. F., Kretchmer J. and Walker D., IEEE Electron Device Letters **23**, 535 (2002).

[17] Lee Y. J., Lee M. H., Cheng C. M. and Yang C. H., Applied Physics Letters **98**, 263504 (2011).

[18] Jani O., Ferguson I., Honsberg C. and Kurtz S., Applied Physics Letters **91**, 132117 (2007).

[19] Wierer J. J., Koleske D. D. and Lee S. R., Applied Physics Letters **100**, 111119 (2012).

[20] Sang L. W., Takeguchi M., Lee W., Nakayama Y., Lozach M., Sekiguchi T. and Sumiya M., Applied Physics Express **3**, 111004 (2010).

[21] Kuwahara Y., Fujii T., Fujiyama Y., Sugiyama T., Iwaya M., Takeuchi T., Kamiyama S., Akasaki I. and Amano H., Applied Physics Express **3**, 111001 (2010).

[22] Rimada J. C., Hernández L., Connolly J. P. and Barnham K. W. J., Microelectronics Journal **38**, 513 (2007).